Role of tryptophan residues of Erv1: Trp95 and Trp183 are important for its folding and oxidase function

Qi Wang[*,†], Swee Kim Ang[*,†,‡], Efrain Ceh-Pavia[*], Jiayun Pang[§] and Hui Lu[*,¶]

[*] *Manchester Institute of Biotechnology, Faculty of Life Sciences, University of Manchester, 131 Princess Street, Manchester M1 7DN, UK*

[‡] *Current address: Department of Microbiology, Yong Loo Lin School of Medicine, National University Health System, 5 Science Drive 2, National University of Singapore, Singapore 117597, Singapore*

[§] *Department of Pharmaceutical, Chemical and Environmental Sciences, Faculty of Engineering and Science, University of Greenwich, Medway Campus, Central Avenue, Chatham Maritime, Kent ME4 4TB, UK*

Short title: Role of Trp residues of Erv1

[†] contributed to the work equally

[¶]To whom correspondence should be addressed: Hui Lu, Manchester Institute of Biotechnology, University of Manchester, 131 Princess Street, Manchester M1 7DN, UK

Tel: +44-161-2751553; Fax: +44-161-3065201; E-mail: hui.lu@manchester.ac.uk

Keywords: sulphydryl oxidase, FAD binding, tryptophan residue, protein folding, mitochondria

Abbreviations:
ALR: augmenter of liver regeneration
Erv: essential for respiration and viability
IMS: intermembrane space;
MIA: mitochondrial import and assembly
TCEP: tris-(2-carboxyethyl) phosphine

SYNOPSIS

Erv1 is an FAD-dependent sulphydryl oxidase of the ERV/ALR sub-family, and an essential component of the mitochondrial import and assembly pathway. Erv1 contains six tryptophan residues, which are all located in the highly conserved C-terminal FAD-binding domain. Though important structural roles were predicted for the invariable Trp95, no experimental study has been reported. In this study, we investigated the structural and functional roles of individual Trp residues of Erv1. Six single Trp-to-Phe yeast mutant strains were generated and their effects on cell viability were tested at various temperatures. Then, the mutants were purified from *E. coli*. Their effects on folding, FAD-binding, and Erv1 activity were characterised. Our results showed that $Erv1^{W95F}$ has the strongest effect on the stability and function of Erv1, and followed by $Erv1^{W183F}$. $Erv1^{W95F}$ results in a decrease of the T_m of Erv1 by 23°C, a significant loss of the oxidase activity, and thus causing cell growth defects at both 30°C and 37°C. $Erv1^{W183F}$ induces changes in the oligomerisation state of Erv1, along with a pronounced effect on the stability of Erv1 and its function at 37°C, whilst the other mutants had no clear effect on the function of Erv1 including the highly conserved Trp157 mutant. Finally, computational analysis indicates that Trp95 plays a key role in stabilising the isoalloxazine ring to interact with Cys133. Taken together, this study provided important insights into the molecular mechanism of how sulfhydryl oxidases use FAD in catalyzing disulfide bond formation. **(245)**

INTRODUCTION

Erv1 (Essential for respiration and viability 1) is an essential component of the mitochondrial import and assembly (MIA) pathway, playing a critical role during import and oxidative folding of the mitochondrial intermembrane space (IMS) proteins [1-3]. In the MIA pathway, Mia40 acts as a sulphydryl oxidoreductase and import receptor, interacting directly with the substrates of the pathway (e.g. Tim9, Tim10, Cox17, and Ccs1). Erv1 is a FAD-dependent sulphydryl oxidase belonging to the single domain ERV/ALR oxidase family. It functions downstream of Mia40, catalysing re-oxidation of the reduced Mia40 and transferring electrons (via FAD) to molecular oxygen and/or cytochrome *c* [4-10].

Saccharomyces cerevisiae Erv1 has a total of 189 amino acids including a highly conserved (among ERV/ALR family) FAD-binding domain of approximately 100 amino acids at the C-terminus (Fig. 1). There are six conserved cysteine residues forming three pairs of disulphide bonds, with four of the cysteine residues located in the FAD-binding domain. Several structures of the FAD-binding domain of ERV/ALR proteins have been published [10-15], in which they are all crystallised as head-to-tail homodimers. Each subunit contains a four-helical bundle (H1-H4) that harbours the FAD cofactor and an additional (5^{th}) single-turn helix (Fig. 1). The FAD-binding domain acts as a catalytic core (also called catalytic domain) containing a CXXC redox centre disulphide (Cys130-Cys133), located proximal to the isoalloxazine ring of FAD cofactor, and a C-terminal $CX_{16}C$ structural disulphide. The shuttle disulphide (Cys30-Cys33) of Erv1 is located in the non-conserved N-terminal domain. It accepts the electrons from reduced Mia40 and transfers them to the active-site disulphide (Cys130-Cys133), and then in turn to the cofactor FAD and cytochrome *c* and/or molecular oxygen [4, 16-19]. Erv1 and ALR employ a similar catalytic mechanism which involves several intermediate states, including a shuttle disulphide reduced state, S→FAD charge-transfer complexes, and an $FADH_2$-Erv1 state, during their catalytic cycle [17, 20-22]. Whilst the shuttle and active-site disulphides are functionally essential, the conserved $CX_{16}C$ disulphide (Cys159-Cys176) plays an important role in stabilising the folding of Erv1[6, 23].

Tryptophan plays important roles in protein stability despite its scarcity in proteins. Erv1 has six Trp residues that are all located in the C-terminal FAD-binding domain making the domain Trp-rich. Among them Trp95, Trp157 and Trp183 are highly conserved across the ERV/ALR family; Trp187 is partially conserved; whilst Trp132 and Trp179 are not conserved (Fig. 1a). Trp95, Trp132 and Trp157 are located in H1, H3 and H4 respectively; Trp179 and Trp183 are in the 5^{th} single-turn helix (H5), and Trp187 is located at the very end of C-terminus, the 3^{rd} residue from the end (Fig. 1a). Interestingly, the highly conserved Trp183 is next to the highly conserved residue Arg182, whose mutation in the human homologue ALR caused diseases. In 2009, Di Fonzo et al. reported the first disease-associated mutant of ALR, in which a single conserved arginine to histidine substitution (ALR^{R194H}) caused an autosomal recessive myopathy [24]. Structural and functional study of the corresponding $Erv1^{R182H}$ mutant showed that Arg182 plays an important role in the folding and FAD binding of Erv1 [25]. Although the oligomerisation state of Erv1 *in vivo* is unclear, our recent *in vitro* study showed that whilst the purified full length Erv1 formed a stable tetramer, the $Erv1^{R182H}$ mutant was a homodimer under the same experimental condition [25]. Visualisation of the structures of Erv1 [11] indicates that both Trp 95 and Trp183 side-chains are involved in stabilising the cofactor binding. Trp95 forms an H-bond with the OH group of the ribitol moiety of FAD, and Trp183 forms an H-bond with the

nitrogen of adenine moiety of FAD using its side chain, suggesting a role similar to Arg182 in stabilising FAD binding. Secondly, both Trp95 and Trp183 seem to play an important part in forming a series of π stackings with the cofactor FAD, involving the isoalloxazine ring of FAD, side chains of Trp95, Tyr128, His162, Phe174, Trp183 and the adenine ring of FAD (Fig. 1c). In particular, the invariable Trp95 of ERV/ALR and Ero1 proteins locates in the centre of the aromatic stacking and is sandwiched between the isoalloxazine ring of FAD and the invariable His162 [11, 13, 26, 27]. Though an important role can be assumed for some of the Trp residues, no experimental study on the importance of the Trp residues and the π stackings in ERV/ALR enzymes' structure and function has been reported.

In the present study, we investigated the structural and functional roles of all six tryptophan residues of Erv1 with a focus on Trp95, using biochemical and biophysical methods, as well as computational and yeast genetic approaches. First, a set of six single tryptophan-to-phenylalanine yeast mutant strains were generated and their effects on cell viability were tested at various temperatures. Then, the Trp mutants were expressed and purified from *E. coli.* Their effects on Erv1 folding, FAD-binding, stability, and oxidase activity were studied using size exclusion chromatography, spectroscopic (absorption, circular dichroism, and FAD fluorescence), and oxygen consumption analyses. Our results show that except Erv1^{W183F}, all mutants were purified as a tetramer like the WT protein, whilst Erv1^{W183F} was a dimer. Erv1^{W95F} has the strongest effect on the stability and hence the function of Erv1, which is followed by Erv1^{W183F}. Though the other mutants also result in observable effects on the folding and stability of Erv1, there is no obvious defect in the oxidase activity of the protein, including the highly conserved Trp157 mutant. Finally, computational analysis was performed to provide insight into the FAD-binding energy landscape at the atomic level, which assisted our understanding of the molecular mechanism by which Erv1^{W95F} causes the functional defect of Erv1.

EXPERIMENTAL PROCEDURES

Site-directed mutagenesis - A construct encoding C-terminally LE(H)$_6$-tagged full-length, wild-type (WT) Erv1 cloned into *Escherichia coli* expression vector pET24a(+) (Novagen) using the Nde1 and Xho1 restriction sites was used as DNA template [28] to generate all mutant constructs for protein purification work in this study. For yeast studies, *ERV1* together with endogenous promoter and terminator regions was inserted into the centromeric plasmid pRS414 as previously described [17] and was used as a DNA template for mutagenesis. Tryptophan-to-phenylalanine mutations were introduced by PCR using overlapping primer pairs containing the desired mutation point. Plasmid DNA constructs with the correct mutation were verified by DNA sequencing.

Protein purification - WT Erv1 and tryptophan mutants were expressed in *E. coli* strain Rosetta-gami™ 2 (Novagen) and purified as previously described [17, 25]. Briefly, protein was expressed in the presence of 0.5 IPTG (mM isopropyl-β-D-1-thiogalactopyranoside) and 10 μM FAD at 16^{o}C for 16-20 hours. Induced cell pellets resuspended in buffer A (150 mM NaCl, 50 mM Tris-HCl, pH 7.4) containing 5 mM imidazole, 50 μM FAD and 1 tablet of EDTA-free protease inhibitor cocktail (Roche) were lysed by sonication on ice. The supernatant fraction containing LE(H)$_6$-tagged Erv1 was bound to 2-3 ml Ni^{2+}-charged His. Bind resin (Novagen) pre-equilibrated with binding buffer. Following a washing step with 20-30 ml of wash buffer (buffer A plus 20 mM imidazole), the protein was eluted with 4-6 ml

of elution buffer (buffer A containing 500 mM imidazole). FAD (100 µM) was added to eluted proteins before storage at -80°C until further use. The affinity-purified proteins were further separated for use in *in vitro* studies by gel filtration chromatography using a Superdex 200 (or Superdex 75) 10/30 column connected to an ÄKTA-FPLC system (GE Healthcare) at 4ºC in BAE (150 mM NaCl, 50 mM Tris-HCl, 1 mM EDTA, pH 7.4).

UV-visible spectroscopy - Absorption spectra were recorded from 250 to 700 nm, at 1 nm intervals, in a 1 cm path-length quartz cuvette using a Cary 300 Bio UV-Visible spectrophotometer (Varian Ltd.). Measurement of the molar extinction coefficient was done in BAE as previously described [6, 7]. The calculated molar extinction coefficients are summarised in Table 1. The FAD content of the WT and mutant Erv1 was calculated based on the equation 1, an extinction coefficient for free FAD of 11.3 mM^{-1} cm^{-1}, and the absorption spectrum of Erv1 or mutants in BAE plus 1%SDS.

$$FAD\% = \frac{\varepsilon 280 * A450}{11.3 * (A280 - 1.82 * A450)} \qquad \text{Eq. 1}$$

ε280 is the extinction coefficient of the apoprotein; 42.54 mM^{-1} cm^{-1} for the WT and 36.85 mM^{-1} cm^{-1} for the single Trp to Phe mutants of Erv1. A280 and A450 are absorbance at 280 and 450 nm respectively. 1.82 is the ratio of ε280/ε450 of free FAD in BAE plus 1% SDS determined in this study.

Circular Dichroism- Circular dichroism (CD) analysis was done using a Chirascan CD spectrometer (Applied Photophysics Ltd.) and either a 1 mm (far UV) or 5 mm (near UV) path-length quartz cuvette. Each spectrum represents an average of four independent scans with the spectra for buffer alone subtracted. Thermal denaturation was measured at 222 nm in 1°C intervals over 5-90°C, with a temperature increase of 1°C/min. Melting temperatures (T_m) were calculated by obtaining the first derivative of each profile and finding the maximum.

Fluorescence spectroscopy- Fluorescence measurements were recorded using a Cary Eclipse fluorescence spectrophotometer (Varian Ltd.) in a 1 cm x 0.2 cm path-length quartz cuvette. Thermal denaturation was followed by the increase in FAD fluorescence at 535 nm after excitation at 455 nm, in 1°C intervals between 5-90°C, with a temperature increase of 1°C/min.

Oxygen consumption assays- Erv1 oxidase activity was measured using a Clark-type oxygen electrode (Hansatech Instrument Ltd, England) in a 0.5 ml reaction volume at 25°C or 37°C in BAE as previously described [6]. Data analysis of the oxygen consumption profile and the calculation of the reaction slope were performed using the Microcal™ Origin™ statistical software package.

Yeast complementation assays - A Δ*erv1* knock-out strain containing WT *ERV1* in a *URA3* plasmid [24] was co-transformed with WT or mutant *ERV1* on *TRP1* plasmid pRS414. For counter-selection tests, the strains were spotted on 5-fluoroorotic acid (FOA) plates and incubated for up to 2-3 days at 25°C, 30°C or 37°C.

Miscellaneous - All experiments were carried out in BAE (150 mM NaCl, 50 mM Tris-HCl, 1 mM EDTA, pH 7.4) unless specifically stated. For multi-angle laser light-scattering, protein samples were applied to a Superdex 200 10/30 gel filtration column (GE Healthcare) running with buffer A. Proteins eluting from the column passed through an in-line DAWN EOS laser photometer set at 682 nm and an Optilab rEX refractor. To calculate the weight-averaged

molecular mass, the light scattering intensity and eluent refractive index were analysed using ASTRA version 4.8 software.

Molecular Dynamics (MD) Simulations - MD simulations of the wild type (WT) and Erv1^{W95F} mutant were performed using AMBER12 [29] with the protein modelled by the AMBER ff99SB force field [30] and the substrate FAD represented using the parameters and partial charges developed by Asada *et al* [31]. The initial protein coordinate was taken from the crystal structure of the C-terminal core domain (CTD) of Erv1 from *Saccharomyces cerevisiae* at 2.0 Å resolution (PDB code: 4E0H) [11]. In the crystal structure, the CTD of Erv1 exists as a homodimer, with each subunit formed of a four-helix bundle that accommodates FAD binding. All crystallographic waters were removed while hydrogens were added using the LEAP program within AMBER12. The protein-FAD complex consisting of 206 amino acid residues (103 residues in each subunit) and two FADs was solvated in a rectangular TIP3P water box with at least 8 Å between the edge of the box and the protein. Chloride ions were added to neutralise the overall change of the system. Following minimisation, the system was heated to 298 K, equilibrated for 200 ps under the constant pressure condition and the production simulation was performed for 1 ns.

Calculation of binding free energy. The MM-GBSA approach [32, 33] implemented in AMBER12 was used to study the FAD binding energy to Erv1 WT (ΔE_{WT}) and Erv1^{W95F} mutant (ΔE_{W95F}). A total of 500 frames from the 1ns MD trajectory were used. The MM–GBSA free energy was obtained from a combination of the gas phase molecular mechanics energy term ($E_{MM} = E_{ele} + E_{vdw} + E_{int}$) and the solvation free energy term ($G_{solvation} = G_{polar} + G_{nonpolar}$) without the solute entropy term. The difference in the energy of FAD binding in the WT and W95F was derived by $\Delta\Delta E = \Delta E_{W95F} - \Delta E_{WT}$.

RESULTS

Effects of Erv1 Trp mutations on yeast cell viability

To investigate the requirement of individual tryptophan residues of Erv1 in its function *in vivo*, we generated six Trp mutant yeast strains by expressing plasmid-encoded *erv1* single Trp to Phe mutants, in an *ERV1* knock-out strain Δ*erv1,* isogenic to the wild-type W303 as described previously [24]. Then, effects of the mutation on the cell viability were checked by spot-testing at 25^{o}C, 30^{o}C and 37^{o}C (Fig. 2). Upon counter-selection of WT *ERV1* (on *URA3*-containing plasmid), the Erv1^{W95F} mutant was temperature sensitive at both 30^{o}C and 37^{o}C, Erv1^{W183F} grew normally at 25^{o}C and 30^{o}C, but slowly at 37^{o}C, whilst the other four mutants showed no obvious growth defect at all three temperatures. This result confirmed that Trp95 and to a lesser extent Trp183 play important roles in the function of Erv1 *in vivo*. The other four Trp residues, including the highly conserved Trp157, were not important for cell viability under these experimental conditions.

Effects of tryptophan mutations on the folding and FAD-binding of Erv1

To understand the structural and functional roles of tryptophan residues of Erv1, six single Trp to Phe mutant constructs of Erv1 were generated and expressed in *E. coli.* All mutants

were successfully purified using the same method as that used for the WT protein, as described previously [6, 17]. Gel filtration chromatography analysis showed that apart from Erv1^{W183F} all other five mutants eluted in the same or similar position as the WT protein, and thus existed mainly in a tetramer form like the WT Erv1 [17, 25] (Fig. 3a; supplementary Fig. S1a). Elution of Erv1^{W183F} was delayed and the molecular weight of Erv1^{W183F} was determined using light scattering analysis to be 44±3 kDa (supplementary Fig. S1b), suggesting that Erv1^{W183F} formed a dimer (monomer Erv1 is 22 kDa).

Though there is a difference in oligomerisation state, all six mutants displayed the same yellowish colour as the WT protein, and showed very similar overall UV-vis absorption spectra profiles (Fig. 3b). The visible absorption maximum λ_{max} was shifted most by Erv1^{W95F}, from 460 nm (for WT) to 458 nm (Table 1). The result suggests that FAD cofactor binding was not significantly affected by the mutation. Consistently, similar extinction coefficients were obtained as shown in Table 1, which were determined by adding of 1% SDS to release FAD as described previously [6, 7]. Moreover, FAD content of each purified mutant was determined (see methods). Apart from Erv1^{W183F} all the other five mutants had ~95% FAD content, very similar compared with the WT Erv1, and thus one FAD per monomer protein. However, the FAD content of Erv1^{W183F} decreased by more than 20%, indicating that Trp183 and possibly also the tetramer formation play a role in stabilising cofactor binding.

Next, far and near UV circular dichroism (CD) analyses were carried out to investigate the effects of the Trp mutants on the folding of Erv1. The spectral profiles were compared to that of the WT protein in relative intensity since they were different in their FAD content and thus holoprotein concentration. The far UV CD spectra (Fig. 4a) were normalised at 208 nm. Overall, all the spectra showed characteristics of highly α-helical conformations, but with some differences in the region from 215 to 240 nm, especially for Erv1^{W95F} and Erv1^{W183F}. Subtraction of the Erv1^{W183F} spectrum from that of the WT gave a bell-shaped peak centred at 230 nm, characteristic of strong aromatic-aromatic interactions (Fig. 4b). In terms of the differences between the WT and Erv1^{W95F} spectra, apart from a positive peak at ~230 nm, there was also a negative peak at ~220 nm suggesting loss of some α-helical structure in Erv1^{W95F}. Similarly, clear differences in the near UV CD spectra between the WT and these two mutants (Erv1^{W95F} and Erv1^{W183F}) were observed (Fig. 4c). The result showed that the peak of Erv1 near UV CD at 285 nm was contributed mainly by Trp95, whilst Trp183 seemed to contribute to the peak at 295 nm significantly. Furthermore, the facts that the near UV CD spectrum of Erv1^{W183F} was closely similar to that of Erv1^{R182H} and that they both formed a dimer (rather than tetramer) indicated that the signal at 295 nm may be associated with formation of a Erv1tetramer.

Taken together, these results showed that both Trp95 and Trp183 are structurally important in folding and FAD binding of Erv1. Whilst Erv1^{W95F} affected the secondary and tertiary structure of Erv1 without affecting its oligomerisation state, Erv1^{W183F} disrupted not only the oligomeric state, but also the secondary structure and tertiary aromatic-aromatic interactions, and decreased FAD content under the experimental conditions.

Effects of the Trp mutations on the stability of Erv1

It has been shown that FAD release and thermal unfolding of Erv1 are a cooperative process [25]. Thus, we investigated how each Trp mutation affects the thermal stability of the protein based on FAD fluorescence intensity change. Firstly, FAD fluorescence spectra of the WT and six mutants and the same concentration of free FAD (fFAD) were recorded at 5°C. As shown in Figure 5a, whilst W95F displayed ~20% fFAD intensity, negligible fluorescence

intensity was detected for the WT and other mutants due to Erv1 binding quenching FAD fluorescence. Secondly, temperature-dependence of FAD fluorescence intensity change, and thus the cofactor release was measured (Fig. 5b), and the results were summarised in Table 1. Apart from W132F, which showed the same midpoints of thermal denaturation (T_m) of 64°C as the WT Erv1, all other five mutants displayed decreased thermal stability. W95F is the most unstable mutant with a T_m of 41°C, which is 23° lower than that of the WT protein. For W183F, T_m of 51°C, a decrease of about 13° was observed (Table 1). W95F had the strongest effect on the stability of Erv1, followed by W183F, W157F, and the non-conserved Trp mutants W179F, W187F, whilst W132F showed no obvious effect on the thermal stability of Erv1 (Fig. 5b, Table 1). This order is not surprising, as the first three residues (W95F, W183F, and W157F) are highly conserved while the last three are not (Fig. 1). Similar T_m values were determined for the mutants based on CD intensity change at 222 nm (Table 1), showing that Erv1 unfolding and cofactor release was a coupled process.

To gain more understanding of the reversibility of the cofactor binding, the FAD fluorescence spectra of the proteins after thermal denaturation were re-recorded at 5°C (Fig. 5c). There was little change to WT Erv1 and fFAD following renaturation. However, clear FAD fluorescence intensity increases were observed for all six mutants (Fig. 5c-d), showing that there was a defect in re-folding and/or cofactor binding in the mutants after thermal denaturation. In summary, consistent with the conclusion above, temperature-dependent studies showed Erv1^{W95F} and Erv1^{W183F} had the strongest effect on the stability of Erv1 and FAD-binding, though all six mutants displayed decreased thermal stability of Erv1.

Effects of Trp mutations on Erv1 oxidase activity

To understand the importance of the Trp residues in Erv1 function, the oxidase activity of the WT and mutants was analysed using oxygen consumption assay with 5 mM TCEP as substrate as established previously [25]. The relative activity of each mutant was calculated based on their initial oxygen consumption rate compared to that of the WT Erv1 (Table 2, Fig. 6a). At 25°C and 30°C, only Erv1^{W95F} showed a clear functional defect, with about 50% activity of the WT Erv1 (Table 2). At 37°C, both Erv1^{W95F} and Erv1^{W183F} displayed a significant functional defect; which Erv1^{W95F} showed ~9% and Erv1^{W183F} had ~53% activity of the WT Erv1 respectively (Fig. 6a). Under the same conditions, the other four mutants, including the highly conserved Trp157 mutant, showed no obvious functional defect, and Erv1^{W187F} was slightly more active than the WT Erv1 at all three temperatures. These results are consistent with our *in vivo* findings and provide a good explanation for the temperature sensitive growth phenotypes we observed (Fig. 2).

Our previous study showed that the Erv1^{R182H}, a disease related mutant, has stronger effects on folding and FAD-binding of the catalytic reaction intermediates of Erv1 than the oxidised steady state enzyme [25]. The cofactor was released readily from Erv1^{R182H} during its catalytic cycle leading to complete inactivation of the enzyme. In the present study, although only ~30% of the oxidised Erv1^{W95F} and 10% of Erv1^{W183F} were denatured at 37°C (Fig. 5b), the activity loss was higher, ~90% and 50% respectively. Thus, we reasoned that similar to Erv1^{R182H} Erv1^{W95F} and Erv1^{W183F} had stronger destabilisation effects on folding and FAD-binding of the reaction intermediates than on the initial oxidised Erv1. To test this hypothesis, the oxygen consumption experiment was carried out in the presence of fFAD. As expected, the oxidase activities of these mutants were recovered by addition of fFAD and in a fFAD concentration dependent manner (Fig. 6b). Moreover, no obvious differences in the stability of the oxidised enzymes were observed based on thermal denaturation studies. T_m of 66±1°C

for the WT and 46±2°C for the W95F mutant were obtained in the presence of 10 uM fFAD, which are the same as those determined in the absence of fFAD (Table 1).

Computational analysis

To understand the effects of W95F mutant on the stability of FAD-binding further, molecular dynamics (MD) simulations (see methods) of the WT and Erv1^{W95F} mutant were performed based on the crystal structure of the C-terminal core domain of Erv1 at 2.0 Å resolution (PDB code: 4E0H) [11]. The overall FAD-binding energies of the WT Erv1 (-71.1±6.0 kcal/mol) and Erv1^{W95F} (-73.7±4.7 kcal/mol), as calculated by the MM-GBSA method, are similar. When the binding energy is decomposed into the contribution of individual residues, key residues that contribute to FAD-binding are identified as shown in Figure 7a and 7b. The residues include Gly91, Arg92, Trp95, Tyr128, Cys133, Phe137, Cys159, His162, Val165, Lys171, Phe174, Arg182 and Trp183. Consistently, these key residues are all located in proximity to and interacting with the isoalloxazine ring, ribitol moiety and adenosine moiety of FAD, respectively (supplementary Fig. S1). However, apparent differences in the contribution of individual residues between the WT and W95F mutant were observed. The residues with significant binding energy changes ($\Delta\Delta E > \pm 0.5$ kcal/mol) are Val87, Arg92, Trp/Phe95, Tyr128, Trp132, Cys133 and Lys171 (Fig. 7c), and interestingly they are all positioned in close proximity to the isoalloxazine ring of FAD (Fig.7d). The result indicates that Trp95 plays a key role in stabilising the isoalloxazine ring in its positioning within the binding site and how it interacts with key residues, such as Cys133 for which the binding energy to FAD is changed by 1.55 kcal/mol in Erv1^{W95F} (Fig. 7c).

DISCUSSION

In this report, we investigated the structural and functional roles of all six tryptophan residues of Erv1, using yeast genetic, biochemical, and computational methods, with focus on the highly conserved Trp95. We showed that all the Trp mutants apart from W132F, had an impact on the thermal stability of Erv1 as evidenced by their decreased Tm (Fig. 5, table 1). In terms of function, the three non-conserved tryptophan residues (Trp132, Trp179 and Trp187) and Trp157, a highly conserved residue in the ERV/ALR sub-family, seem not to be essential for Erv1 function under normal cell growth or our experimental conditions (Fig. 1, Table 2). However, both Trp95 and Trp183 play an important role in stabilising the folding and FAD-binding, and thus the function of Erv1.

Mutagenesis studies of several FAD/FMN-dependent enzymes suggested that aromatic residues forming π stacking interactions with the isoalloxazine ring of FAD/FMN help stabilise formation of the anionic flavin hydroquinone intermediate [34-36]. Similarly, in our study, mutating Trp95 into Phe affects the π- π repulsive interactions between the ring systems, which may modulate the catalytic steps for the formation of the S→FAD charge-transfer complexes. Our experimental results showed that Erv1^{W95F} has the strongest effect on the stability and oxidase activity of Erv1. The functional defect of Erv1^{W95F} is largely due to the destabilising effects on the catalytic reaction intermediates since its activity can be recovered and sustained by addition of free FAD in the reaction. This observation is consistent with the result of our computational analysis, suggesting that Trp95 is crucial in stabilising the isoalloxazine ring to interact with Cys133, hence the redox centre disulphide. Consequently, Erv1^{W95F} mutation causes a strong functional defect of Erv1 and impaired cell growth at both 30°C and 37°C.

Trp183, on the other hand, is not directly involved in the π stacking network, and only forms an H-bond with the nitrogen of adenine moiety of FAD. This serves to maintain the orientation of the adenine ring (FAD is in a bent conformation with the isoalloxazine and the adenine ring buried in the active site and sandwiched between Trp95 and His162). Therefore, mutating Trp183 to Phe is not as severe as W95F in terms of its effect on Erv1 oxidase function (Table 2). However, $Erv1^{W183F}$ showed a significant effect on the oligomerisation state of Erv1, which leads to a clear functional and growth defect at 37°C but not at 30°C. This result is the same as that caused by $Erv1^{R182H}$, a disease related mutant, forming a dimer under the same experimental conditions [25]. The fact that both Arg182 and Trp183 are part of the 5th single turn α-helix (H5) of Erv1 shows that this region is important in stabilising the tetramer formation. Furthermore, Arg182 may form intermolecular hydrogen bonds to stabilise the tetramer formation, which may be assisted by a typical side-chain cation-π interaction with Trp183. Since Trp is more favoured to interact with cationic side-chains than Phe [37], we hypothesise that mutation of Trp183 disrupts the cation-π interaction with Arg182, causing disruption of the intermolecular interactions mediated by Arg182, and subsequent dissociation of the tetrameric structure of Erv1. Such a molecular mechanism of oligomerisation formation has been observed previously [38]. Together with the observation that purified W183F mutant showed a decreased FAD content than the WT and other Trp mutants (Table 1), our results suggest that tetramer formation plays an important role in stabilising the cofactor binding by Erv1 through the cation-π interaction between Arg182 and Trp183 and Trp183's contribution in maintaining the π-π stacking network.

More generally, the aromatic ring stacking is conserved not only in ERV/ALR family, but all FAD-dependent sulfhydryl oxidases, including Ero1 (a sulfhydryl oxidase of the endoplasmic reticulum) that has no sequence homology with ERV/ALR enzymes [26, 27, 39]. Thus, it is tenable that the extensive π-π stacking around FAD is the key to create a rigid active site to receive electrons from the active-site disulphide (Cys130-Cys133) and pass electrons to molecular oxygen. Taken together, the current study contributes to our understanding of how sulfhydryl oxidases use FAD to catalyze the disulfide bond formation and broadly, provide insights into the function and mechanism of the structurally diverse flavinenzymes.

ACKNOWLEDGEMENT

We thank Marjorie Howard of the faculty biomolecular analysis core facility for help with light scattering measurement; to John Milward and Abid Javed for initial preliminary work, to Michael Spiller for advice on yeast genetics, to Andy Munro and Derren Heyes for helpful comments on the manuscript. Research by HL group was supported by the Biotechnology and Biological Sciences Research Council (BBSRC) (BB/H017208) and the Leverhulme Trust (F/00120/CB). JP would like to acknowledge computational power provided by the UK Engineering and Physical Sciences Research Council (EPSRC), the UK National Service for Computational Chemistry Software (NSCCS) and the UK High-End Computing Consortium for Biomolecular Simulation (HECBioSim). The authors declare that they have no conflict of interest.

REFERENCES

1. Riemer, J., Fischer, M. and Herrmann, J. M. (2011) Oxidation-driven protein import into mitochondria: Insights and blind spots. Biochim Biophys Acta. **1808**, 981-989.

2. Sideris, D. P. and Tokatlidis, K. (2010) Oxidative protein folding in the mitochondrial intermembrane space. Antioxid Redox Signal. **13**, 1189-1204.
3. Chacinska, A., Koehler, C. M., Milenkovic, D., Lithgow, T. and Pfanner, N. (2009) Importing mitochondrial proteins: machineries and mechanisms. Cell. **138**, 628-644.
4. Lionaki, E., Aivaliotis, M., Pozidis, C. and Tokatlidis, K. (2010) The N-terminal shuttle domain of Erv1 determines the affinity for Mia40 and mediates electron transfer to the catalytic Erv1 core in yeast mitochondria. Antioxid. Redox Signal. **13**, 1327-1339.
5. Bien, M., Longen, S., Wagener, N., Chwalla, I., Herrmann, J. M. and Riemer, J. (2010) Mitochondrial disulfide bond formation is driven by intersubunit electron transfer in Erv1 and proofread by glutathione. Mol Cell. **37**, 516-528.
6. Ang, S. K. and Lu, H. (2009) Deciphering structural and functional roles of individual disulfide bonds of the mitochondrial sulfhydryl oxidase Erv1p. J Biol Chem. **284**, 28754-28761.
7. Dabir, D. V., Leverich, E. P., Kim, S. K., Tsai, F. D., Hirasawa, M., Knaff, D. B. and Koehler, C. M. (2007) A role for cytochrome c and cytochrome c peroxidase in electron shuttling from Erv1. Embo J. **26**, 4801-4811.
8. Bihlmaier, K., Mesecke, N., Terziyska, N., Bien, M., Hell, K. and Herrmann, J. M. (2007) The disulfide relay system of mitochondria is connected to the respiratory chain. J Cell Biol. **179**, 389-395.
9. Daithankar, V. N., Farrell, S. R. and Thorpe, C. (2009) Augmenter of liver regeneration: substrate specificity of a flavin-dependent oxidoreductase from the mitochondrial intermembrane space. Biochemistry. **48**, 4828-4837.
10. Allen, S., Balabanidou, V., Sideris, D. P., Lisowsky, T. and Tokatlidis, K. (2005) Erv1 mediates the Mia40-dependent protein import pathway and provides a functional link to the respiratory chain by shuttling electrons to cytochrome c. J Mol Biol. **353**, 937-944.
11. Guo, P. C., Ma, J. D., Jiang, Y. L., Wang, S. J., Bao, Z. Z., Yu, X. J., Chen, Y. and Zhou, C. Z. (2012) Structure of yeast sulfhydryl oxidase erv1 reveals electron transfer of the disulfide relay system in the mitochondrial intermembrane space. J Biol Chem. **287**, 34961-34969.
12. Wu, C. K., Dailey, T. A., Dailey, H. A., Wang, B. C. and Rose, J. P. (2003) The crystal structure of augmenter of liver regeneration: A mammalian FAD-dependent sulfhydryl oxidase. Protein Sci. **12**, 1109-1118.
13. Gross, E., Sevier, C. S., Vala, A., Kaiser, C. A. and Fass, D. (2002) A new FAD-binding fold and intersubunit disulfide shuttle in the thiol oxidase Erv2p. Nat Struct Biol. **9**, 61-67.
14. Vitu, E., Bentzur, M., Lisowsky, T., Kaiser, C. A. and Fass, D. (2006) Gain of function in an ERV/ALR sulfhydryl oxidase by molecular engineering of the shuttle disulfide. J Mol Biol. **362**, 89-101.
15. Daithankar, V. N., Schaefer, S. A., Dong, M., Bahnson, B. J. and Thorpe, C. (2010) Structure of the human sulfhydryl oxidase augmenter of liver regeneration and characterization of a human mutation causing an autosomal recessive myopathy. Biochemistry. **49**, 6737-6745.
16. Mesecke, N., Terziyska, N., Kozany, C., Baumann, F., Neupert, W., Hell, K. and Herrmann, J. M. (2005) A disulfide relay system in the intermembrane space of mitochondria that mediates protein import. Cell. **121**, 1059-1069.
17. Ang, S. K., Zhang, M., Lodi, T. and Lu, H. (2014) Mitochondrial sulphydryl oxidase Erv1: both shuttle cysteine residues are required for its function with distinct roles. Biochem J. **460**, 199-210.

18. Rissler, M., Wiedemann, N., Pfannschmidt, S., Gabriel, K., Guiard, B., Pfanner, N. and Chacinska, A. (2005) The essential mitochondrial protein Erv1 cooperates with Mia40 in biogenesis of intermembrane space proteins. J Mol Biol. **353**, 485-492.
19. Tienson, H. L., Dabir, D. V., Neal, S. E., Loo, R., Hasson, S. A., Boontheung, P., Kim, S. K., Loo, J. A. and Koehler, C. M. (2009) Reconstitution of the mia40-erv1 oxidative folding pathway for the small tim proteins. Mol Biol Cell. **20**, 3481-3490.
20. Banci, L., Bertini, I., Calderone, V., Cefaro, C., Ciofi-Baffoni, S., Gallo, A. and Tokatlidis, K. (2012) An electron-transfer path through an extended disulfide relay system: the case of the redox protein ALR. J Am Chem Soc. **134**, 1442-1445.
21. Kodali, V. K. and Thorpe, C. (2010) Oxidative protein folding and the Quiescin-sulfhydryl oxidase family of flavoproteins. Antioxid Redox Signal. **13**, 1217-1230.
22. Schaefer-Ramadan, S., Gannon, S. A. and Thorpe, C. (2013) Human augmenter of liver regeneration: probing the catalytic mechanism of a flavin-dependent sulfhydryl oxidase. Biochemistry. **52**, 8323-8332.
23. Kallergi, E., Andreadaki, M., Kritsiligkou, P., Katrakili, N., Pozidis, C., Tokatlidis, K., Banci, L., Bertini, I., Cefaro, C., Ciofi-Baffoni, S., Gajda, K. and Peruzzini, R. (2012) Targeting and maturation of Erv1/ALR in the mitochondrial intermembrane space. ACS Chem Biol. **7**, 707-714.
24. Di Fonzo, A., Ronchi, D., Lodi, T., Fassone, E., Tigano, M., Lamperti, C., Corti, S., Bordoni, A., Fortunato, F., Nizzardo, M., Napoli, L., Donadoni, C., Salani, S., Saladino, F., Moggio, M., Bresolin, N., Ferrero, I. and Comi, G. P. (2009) The mitochondrial disulfide relay system protein GFER is mutated in autosomal-recessive myopathy with cataract and combined respiratory-chain deficiency. Am J Hum Genet. **84**, 594-604.
25. Ceh-Pavia, E., Ang, S. K., Spiller, M. P. and Lu, H. (2014) The disease-associated mutation of the mitochondrial thiol oxidase Erv1 impairs cofactor binding during its catalytic reaction. Biochem J. **464**, 449-459.
26. Gross, E., Kastner, D. B., Kaiser, C. A. and Fass, D. (2004) Structure of Ero1p, source of disulfide bonds for oxidative protein folding in the cell. Cell. **117**, 601-610.
27. Fass, D. (2008) The Erv family of sulfhydryl oxidases. Biochim Biophys Acta. **1783**, 557-566.
28. Lee, J., Hofhaus, G. and Lisowsky, T. (2000) Erv1p from *Saccharomyces cerevisiae* is a FAD-linked sulfhydryl oxidase. FEBS Lett. **477**, 62-66.
29. Case, D., Darden, T., Cheatham III, T., Simmerling, C., Wang, J., Duke, R., Luo, R., Walker, R., Zhang, W. and Merz, K. (2012) AMBER 12. ed.)^eds.), University of California, San Francisco.
30. Hornak, V., Abel, R., Okur, A., Strockbine, B., Roitberg, A. and Simmerling, C. (2006) Comparison of multiple Amber force fields and development of improved protein backbone parameters. Proteins. **65**, 712-725.
31. Asada, T., Nagase, S., Nishimoto, K. and Koseki, S. (2008) Molecular dynamics simulation study on stabilities and reactivities of NADH cytochrome B5 reductase. The journal of physical chemistry. B. **112**, 5718-5727.
32. Kollman, P. A., Massova, I., Reyes, C., Kuhn, B., Huo, S., Chong, L., Lee, M., Lee, T., Duan, Y., Wang, W., Donini, O., Cieplak, P., Srinivasan, J., Case, D. A. and Cheatham, T. E., 3rd. (2000) Calculating structures and free energies of complex molecules: combining molecular mechanics and continuum models. Acc Chem Res. **33**, 889-897.
33. Ivanova, E., Pang, J., Jowitt, T. A., Yan, G., Warwicker, J., Sutcliffe, M. J. and Lu, H. (2011) Temperature-dependent study reveals that dynamics of hydrophobic residues plays an important functional role in the mitochondrial Tim9-Tim10 complex. Proteins. **80**, 602-615.

34. Pellett, J. D., Becker, D. F., Saenger, A. K., Fuchs, J. A. and Stankovich, M. T. (2001) Role of aromatic stacking interactions in the modulation of the two-electron reduction potentials of flavin and substrate/product in Megasphaera elsdenii short-chain acyl-coenzyme A dehydrogenase. Biochemistry. **40**, 7720-7728.
35. Zhou, Z. and Swenson, R. P. (1996) The cumulative electrostatic effect of aromatic stacking interactions and the negative electrostatic environment of the flavin mononucleotide binding site is a major determinant of the reduction potential for the flavodoxin from Desulfovibrio vulgaris [Hildenborough]. Biochemistry. **35**, 15980-15988.
36. Bresnahan, C. G., Reinhardt, C. R., Bartholow, T. G., Rumpel, J. P., North, M. and Bhattacharyya, S. (2015) Effect of stacking interactions on the thermodynamics and kinetics of lumiflavin: a study with improved density functionals and density functional tight-binding protocol. The journal of physical chemistry. A. **119**, 172-182.
37. Gallivan, J. P. and Dougherty, D. A. (1999) Cation-pi interactions in structural biology. Proc Natl Acad Sci U S A. **96**, 9459-9464.
38. Wu, D., Hu, Q., Yan, Z., Chen, W., Yan, C., Huang, X., Zhang, J., Yang, P., Deng, H., Wang, J., Deng, X. and Shi, Y. (2012) Structural basis of ultraviolet-B perception by UVR8. Nature. **484**, 214-219.
39. Thorpe, C., Hoober, K. L., Raje, S., Glynn, N. M., Burnside, J., Turi, G. K. and Coppock, D. L. (2002) Sulfhydryl oxidases: emerging catalysts of protein disulfide bond formation in eukaryotes. Arch Biochem Biophys. **405**, 1-12.

Table 1: Summary of the properties of FAD-binding and stability of the WT and mutant Erv1. The parameters were determined in BAE at pH 7.4 under the same conditions for all proteins as described in the Methods section. [a.] T_m determined based on FAD fluorescence; [b.] T_m determined based on CD at 222 nm. Errors represent means ± SE, n≥2.

Erv1	λ_{max}(nm)	ε ($mM^{-1}cm^{-1}$)	FAD%	T_m (°C)[a]	T_m (°C)[b]
WT	460±1	12.3	95±3	64±2	66±2
W95F	458±2	11.8	93±5	42±2	45±3
W132F	460±1	12.2	94±3	64±2	65±2
W157F	460±1	12.3	92±3	54±2	55±2
W179F	460±1	12.3	100±3	57±2	56±2
W183F	459±1	11.6	71±3	51±2	50±2
W187F	461±1	11.7	94±3	59±2	58±2

Table 2: Oxidase activity and cell viability of the WT and mutant Erv1. The activities were determined based on the initial oxygen consumption rate using that of the WT as 100%. Oxygen consumption catalysed by 3 uM of the WT or a Trp mutant using 5 mM TCEP as the electron donor in the presence of SOD as described in the Methods section. Errors represent means ± SE, n≥3.The cell growth phenotypes were determined based on spot-test shown in Figure 7.

Erv1	Activity @ 25°C	Activity @ 30°C	Activity @ 37°C	Cell viability
WT	100	100	100	WT
W95F	53±7	46±5	9±5	ts @ 30°C& 37°C
W132F	90±8	107±5	99±2	WT-like
W157F	84±4	109±12	98±2	WT-like
W179F	95±4	99±5	102±5	WT-like
W183F	102±7	112±5	53±5	ts @ 37°C
W187F	108±2	128±5	118±5	WT-like

FIGURE LEGENDS

Fig. 1: Cell viability of the Erv1 WT and Trp mutant strains. Yeast complementation assays with Trp mutant Erv1 expression via plasmid shuffling in the absence and presence of 5-fluoroorotic acid (FOA). Strains containing empty vector or Erv1 WT were used as negative and positive controls respectively. Cells were grown at 25°C, 30°C, or 37°C for 2-3 days.

Fig. 2: Sequence alignment of ERV/ALR homologues and structure of Erv1. (**a**) Sequence alignment of Erv/ALR proteins. *Sc*: *Sacharomyces cerevisiae*, *Hs*: *Homo sapiens*, *Rn*: *Rattus norvegicus*, *At*: *Arabidopsis thaliana*. Trp residues are highlighted in grey and numbered for yeast Erv1. (**b**) The X-ray crystal structure of yeast Erv1 core domain residues 84-188 with FAD and the six Trp residues shown (PDB code: 4E0OH) [11]. The structures were generated using the PyMOL VMD software. **(c)** Zoomed in structure of Erv1 showing how Trp95 is involved in both H-bonds and π-stacking interactions to stabilise FAD binding.

Fig. 3: Oligomerisation state and absorption spectra of the WT and Trp mutants of Erv1. (a) Gel filtration chromatography profiles of the WT (black line) and six Trp mutants (as indicated) on a Superdex 200 column. (**b).** UV-visible spectra of the WT and Trp mutants.

Fig. 4: CD spectra of the WT and Trp mutants of Erv1. (a) Far UV CD spectra of 10 μM the WT (black line) and Trp mutants. **(b)** Different spectra of the far UV CD spectra obtained by subtraction of the mutant CD spectrum from that of the WT in (a). **(c)** Near UV CD spectra of the WT and Trp mutants of Erv1. All the colours were used systematically as in Fig. 1.

Fig. 5: FAD fluorescence spectra and thermal stability of the WT and Trp mutants of Erv1. (a, c) 10 μM FAD fluorescence spectra of the WT, Trp mutants, and free FAD (fFAD) measured at 5°C before (a) and after (c) thermal denaturation as shown in (b). (**b**) Thermal denaturation of the WT and mutant proteins followed by FAD fluorescence with excitation at 450 nm and emission at 527 nm. (**d**). Relative total FAD fluorescence intensity (450-650 nm) of the proteins before (black) and after (grey) thermal denaturation normalised to that of fFAD as 100%.

Fig. 6: Oxidase activity of the WT and Trp mutants of Erv1. (**a**) The relative activities of the WT and six Trp mutants of Erv1 measured based on oxygen consumption at 37ºC. The activities were normalised to that of the WT Erv1 as 100%. All reactions contained 3 μM of the WT or mutant protein, using 5 mM TCEP as the electron donor in the presence of SOD. The initial rates of oxygen consumption were used to calculate the relative activities. Errors represent means ± SE, n≥3. (**b**) Time courses of oxygen consumption at 37ºC catalysed by 1 μM of WT with/without addition of 100 μM free FAD (fFAD) or 1 μM W95F mutant in the presence of various fFAD concentrations as indicated in the figure.

Fig. 7: Computational analysis. (a) Decomposition of the total FAD-binding energy into the contribution of individual residues for the WT Erv1, and **(b)** the decomposition plot for $Erv1^{W95F}$. **(c)** Changes in the energy of FAD binding by individual residues in the WT and W95F ($\Delta\Delta E = \Delta E^{W95F} - \Delta E^{WT}$). Residues with ΔΔE greater than ±0.5 kcal/mol are labelled. **(d)** Zoomed in structure of Erv1 showing residues whose binding energies to FAD are perturbed the most ($|\Delta\Delta E|>0.5$ kcal/mol) by the W95F mutation as shown in (c).

Wang et al. Figure 1

a

```
ScErv1     MKAIDKMTDNP----------PQEGLSGRKIIYDEDGKPCRSCNT---LLDFQYVTGKIS 47
HsALR      MAAPGERGRFHGGNLF-FLPGGARSEMMDDLATDARGRGAGRRDAAASASTPAQAPTSDS 59
RnALR      MAAPSEPAGFPRGSRFSFLPGGARSEMTDDLVTDARGRGARHRDD----TTPAAAPAPQG 56
AtErv1     ----------------------MGEKPWQPLLQSFEKLSNCVQTHLSNFIGIKNTPPSSQ 38

                                                          95
ScErv1     NGLKNLSSNGKLAGTGALTGEASELMPGSRTYRKVDPPDVEQLGRSSWTLLHSVAASYPA 107
HsALR      PVAEDASRRRPCRACVDFKTWMRTQQKRDTKFREDCPPDREELGRHSWAVLHTLAAYYPD 119
RnALR      --LEHG--KRPCRACVDFKSWMRTQQKRDIKFREDCPQDREELGRHTWAFLHTLAAYYPD 112
AtErv1     STIQNP--IISLDSSPPIATNSSSLQKLPLKDKSTGPVTKEDLGRATWTFLHTLAAQYPE 96

                                 132                          157
ScErv1     QPTDQQKGEMKQFLNIFSHIYPCNWCAKDFEKYIRENAPQVESREELGRWMCEAHNKVNK 167
HsALR      LPTPEQQQDMAQFIHLFSKFYPCEECAEDLRKRLCRNHPDTRTRACFTQWLCHLHNEVNR 179
RnALR      RPTPEQQQDMAQFIHIFSKFYPCEECAEDIRKRIGRNQPDTSTRVSFSQWLCRLHNEVNR 172
AtErv1     KPTRQQKKDVKELMTILSRMYPCRECADHFKEILRSNPAQAGSQEEFSQWLCHVHNTVNR 156

                      179  183  187
ScErv1     KLRKPKFDCNFWEKRW-KDGWDE---------------- 189
HsALR      KLGKPDFDCSKVDERW-RDGWKDGSCD------------ 205
RnALR      KLGKPDFDCSRVDERW-RDGWKDGSCD------------ 198
AtErv1     SLGKLVFPCERVDARWGKLECEQKSCDLHGTSMDF---- 191
```

b

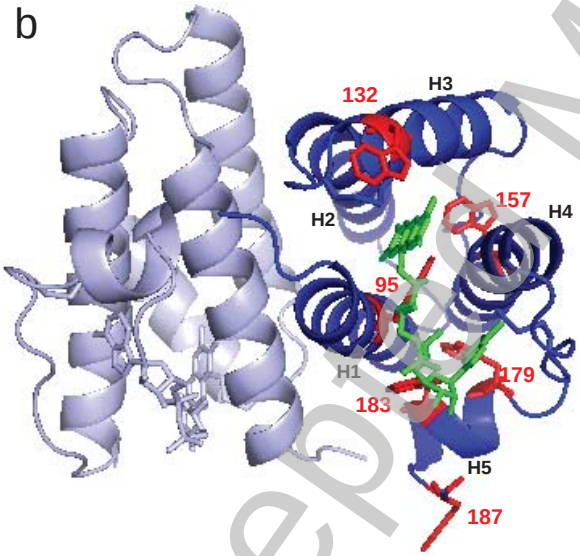

c

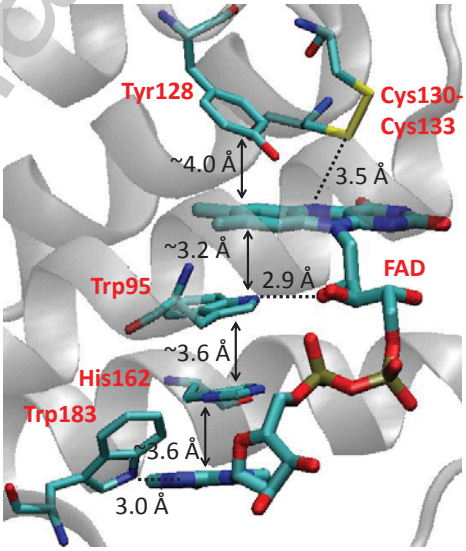

Wang et al. Figure 2

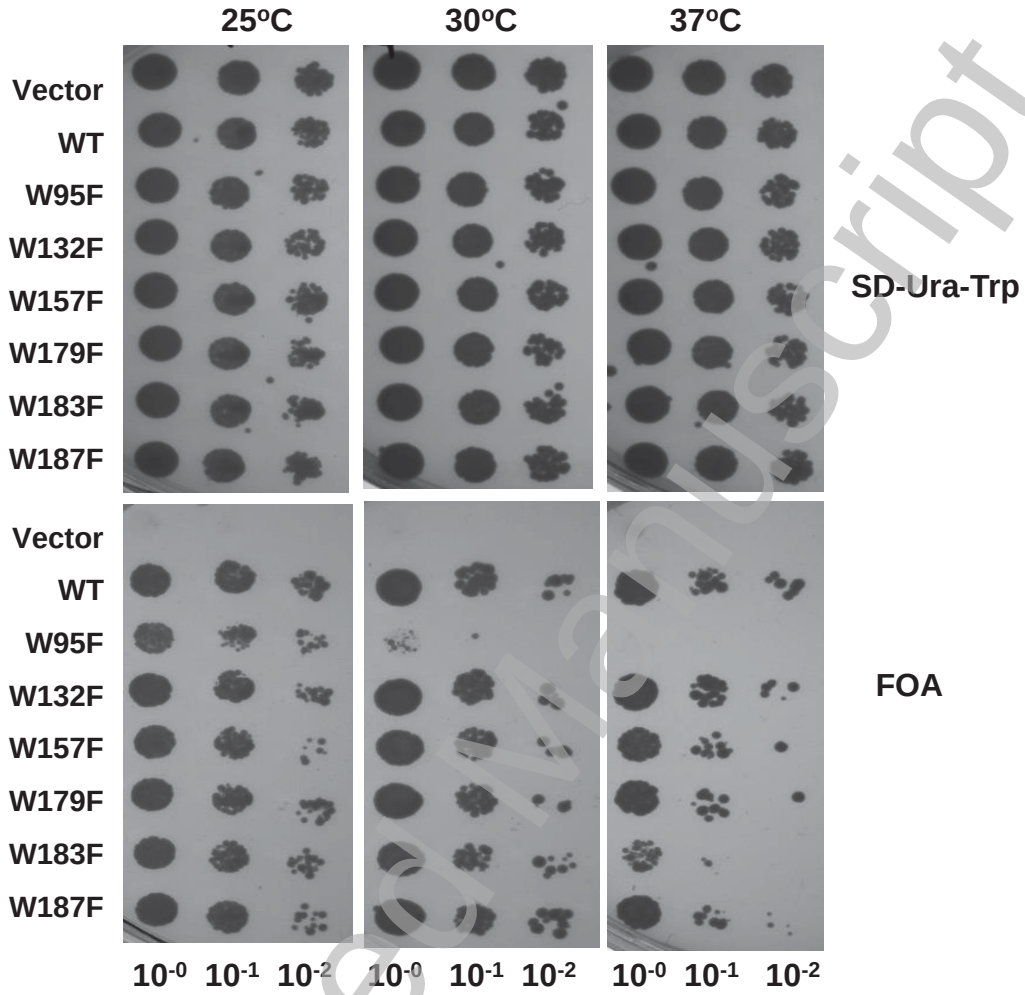

Wang et al. Figure 3

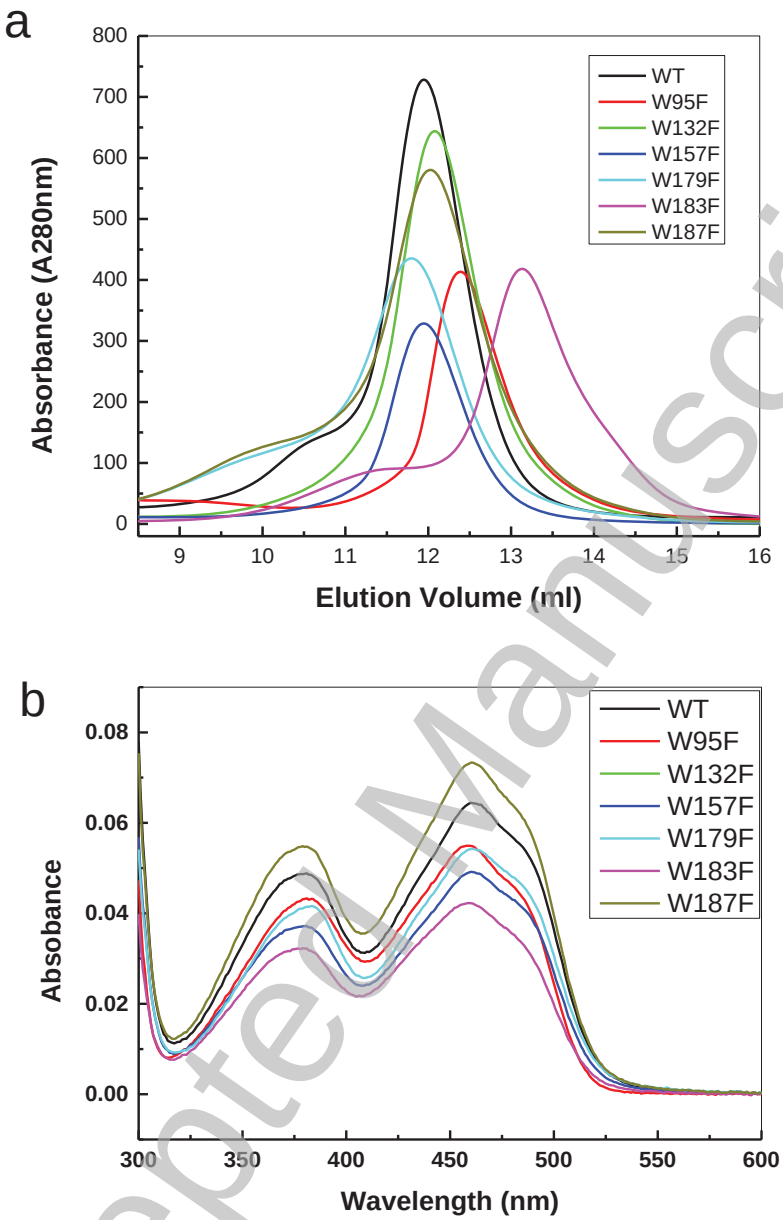

Wang et al. Figure 4

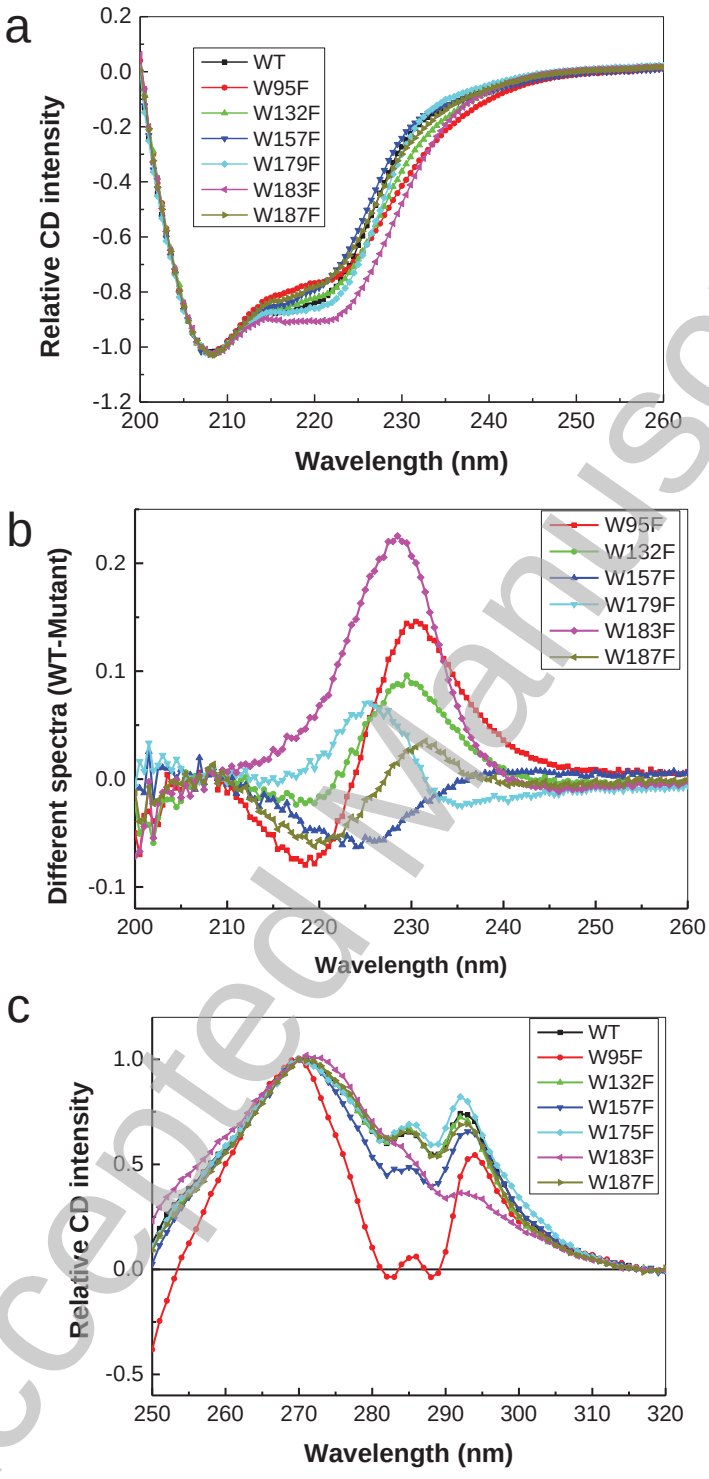

Wang et al. Figure 5

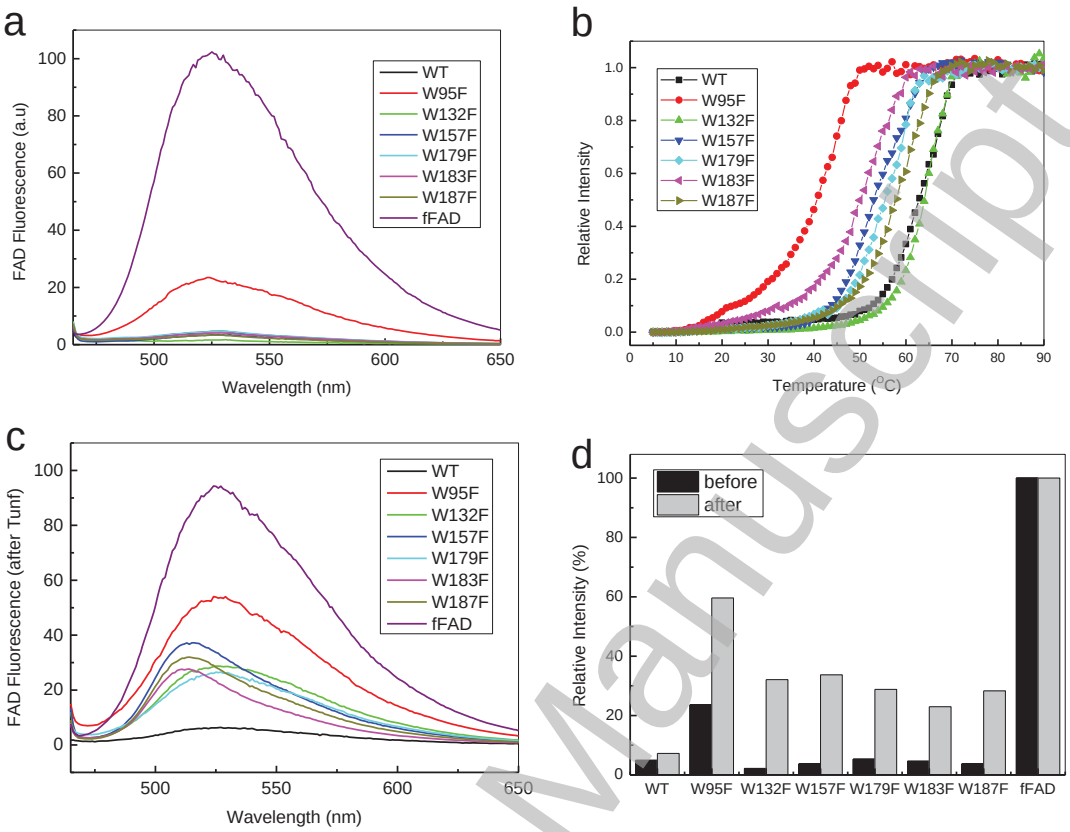

Wang et al. Figure 6

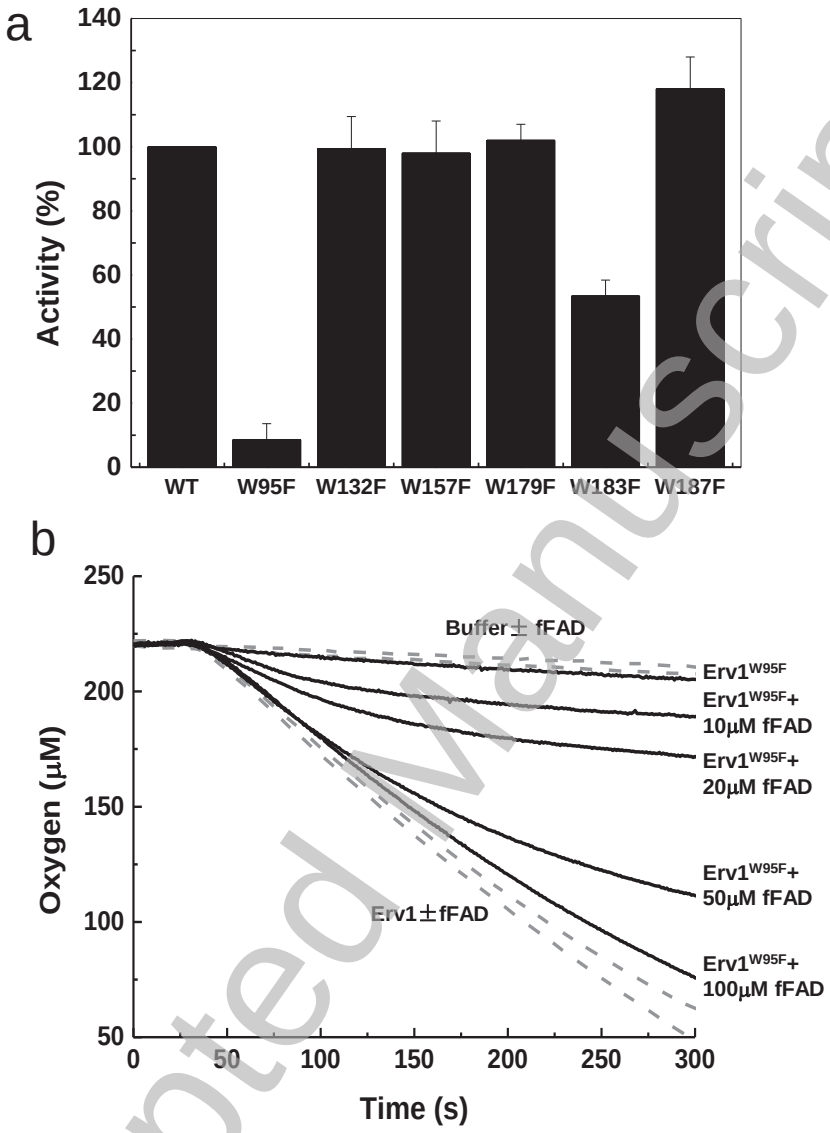

Wang et al. Figure 7